

**DUST-DRIVEN POLAR VORTEX DYNAMICS AND SNOWFALL FROM MARS CLIMATE SOUNDER OBSERVATIONS.** N. R. Alsaeed<sup>1</sup>, P. O. Hayne<sup>1</sup>, and V. Concepcion<sup>1</sup>. <sup>1</sup>Laboratory for Atmospheric and Space Physics, University of Colorado, Boulder CO 80309 (noora.alsaeed@colorado.edu).

**Introduction:** The polar regions on Mars play an important role in the thermal regulation and circulation of the atmosphere. In the winter, strong westerly jets isolate the cold air above the poles from lower latitudes. This aptly named polar vortex inhibits transport of dust and other condensates into the poles [1,2]. Temperatures within the polar vortex boundary drop to the freezing point of carbon dioxide, allowing it to condense out both directly onto the surface and as snowfall [3]. As it is the main constituent of the Martian atmosphere, the surface-atmosphere exchange of CO<sub>2</sub> is one of the fundamental processes in both the present and past climate on Mars, mainly due to its ability to significantly alter the atmospheric pressure and heat balance of the planet on seasonal and orbital timescales [4,5]. It is therefore important to understand what forces affect the dynamics of the polar vortex and subsequently the atmospheric processes that occur within it.

In this work we use atmospheric retrievals of temperature and CO<sub>2</sub> ice cloud opacity from the Mars Climate Sounder (MCS) on board NASA's Mars Reconnaissance Orbiter (MRO) to analyze patterns in the winter polar vortex and CO<sub>2</sub> ice clouds over the north pole for Mars years (MY) 29 to 34. We also couple the MCS data with a simple snowfall model to determine precipitation rates of CO<sub>2</sub> snow.

**Data and Methods:** We use data from MCS, an infrared radiometer that measures the thermal emission of the atmosphere to retrieve vertical profiles of temperature, dust, water vapor and other condensates [6]. In this work we use retrievals of the pressure, temperature, and dust opacity [7] which is converted to CO<sub>2</sub> ice opacity as described in [8]. We limit the data to the northern polar winter between  $L_s = 180^\circ$  and  $360^\circ$  with latitudes above 65 N for MY 29 to 34. For each  $L_s$  in each year, we convert the CO<sub>2</sub> opacities to CO<sub>2</sub> density profiles, and use different binning procedures in latitude and longitude to parse out patterns in the data.

In our analysis of the polar vortex, we bin the temperature between 10 and 20 km above the surface into 5-degree latitude and longitude bins for each  $L_s$  and define the vortex boundary at  $T = 170$  K. We do this for the entirety of northern winter for all Mars years between MY 29 and 34 and observe changes in the area covered by the polar vortex over the seasonal and annual timescales. Results are shown in Figure 2.

For the snowfall analysis, we input the CO<sub>2</sub> profiles into a snowfall model to track deposition onto the surface. The snowfall model we use is a cloud settling model described by a Fokker-Planck-Smoluchowski

diffusion equation which incorporates both diffusion and gravitational settling of the ice particles [9]. We aggregate the snowfall amounts over the entire winter season for each Mars year.

**Results and Discussion:** In our analysis, three patterns emerge: 1) Strong coupling between dust activity in the southern hemisphere and polar vortex dynamics in the northern polar winter. 2) Increased snowfall rates with dust activity, with enhanced snowfall rates in lower latitudes during global dust storms. 3) A persistent longitudinal stationary wave in CO<sub>2</sub> ice cloud densities within the polar vortex.

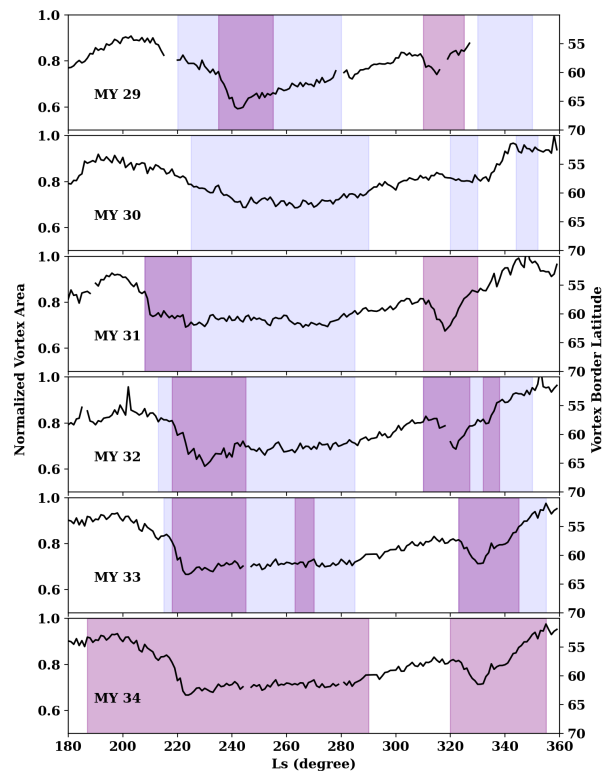


**Figure 1:** Northern polar vortex area, given as a fraction of the total area encompassed above 50 N, for MY 29 to 34. The light blue shaded areas correspond to weaker dust events where the dust opacity (scaled to 610 Pa) was larger than 0.25, and darker purple areas correspond to stronger dust events where the dust opacity was larger than 0.375. The polar vortex boundary is defined to be at  $T = 170$  K. Dust information was sourced from the Mars Climate Database [10].

*Polar vortex coupling with dust activity.* Unlike the polar vortex on Earth, which grows during the winter season, the northern polar vortex on Mars shrinks in size multiple times throughout the winter [2]. As described in previous work by others [11, 12], this shrinking is due

to the presence of a dust cycle on Mars. Figure 1 shows the strong coupling between dust events in the southern Hemisphere and the shrinking of the polar vortex in the northern pole. We observe that the reduction in size of the polar vortex is also coupled with cooler temperatures within the vortex, and enhanced snowfall amounts as shown in Figure 2.

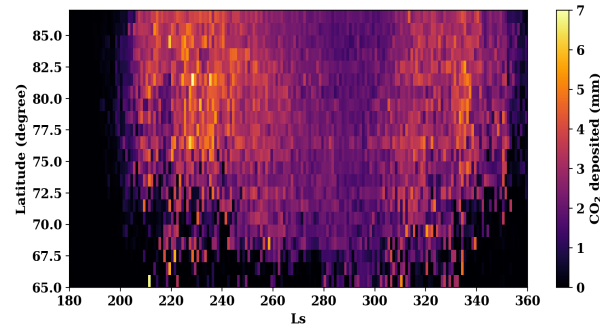


**Figure 2:** CO<sub>2</sub> snowfall deposition per latitude onto the northern polar surface as a function of  $L_s$ . Plotted values are the median deposition for MY 29 to 33.

*Snowfall enhancement with dust activity.* Our results show active snowfall throughout the entirety of the northern winter season, with slight year to year variation in the total amounts of snowfall as shown in table 1. The effects of the dust events are also illustrated in Figure 2, where there is a clear enhancement in the amount of snowfall at  $L_s$  220° and at  $L_s$  320°. These timeframes align with the categorized B and C dust storms that kick off in the southern hemisphere [13].

**Table 1:** Total CO<sub>2</sub> ice deposition due to snowfall at the end of northern winter.

| Mars Year | CO <sub>2</sub> ice mass deposited (kg) | CO <sub>2</sub> ice equivalent thickness (cm) |
|-----------|---|---|
| 29        | 4e15                                    | 40  |
| 30        | 3.7e15                                  | 39  |
| 31        | 3.9e15                                  | 40  |
| 32        | 3.5e15                                  | 37  |
| 33        | 3.2e15                                  | 33  |
| 34        | 3.7e15                                  | 37  |

We also found that the planet-encircling dust storm of MY 34 caused even further enhancement in the snowfall rates, but only in lower latitudes of the polar vortex. This is likely due to two factors: a) the global dust storm allowed more dust to be injected into the

polar vortex area at its boundary (lower latitudes) which served as condensation nuclei for CO<sub>2</sub> ice to precipitate out. b) the larger presence of suspended dust increases the cooling rate of the atmosphere in the polar night [9], causing more CO<sub>2</sub> to condense.

*Longitudinal stationary wave.* Within the polar vortex region, a clear longitudinal wave pattern emerges in the density of the CO<sub>2</sub> clouds, as seen in Figure 3. This pattern is persistent from one Mars year to the next and enhances during the global dust storm in MY 34. The stationary planetary wave is likely a forced oscillation driven by topography [14], which possibly affects the ellipticity of the vortex as well [2].

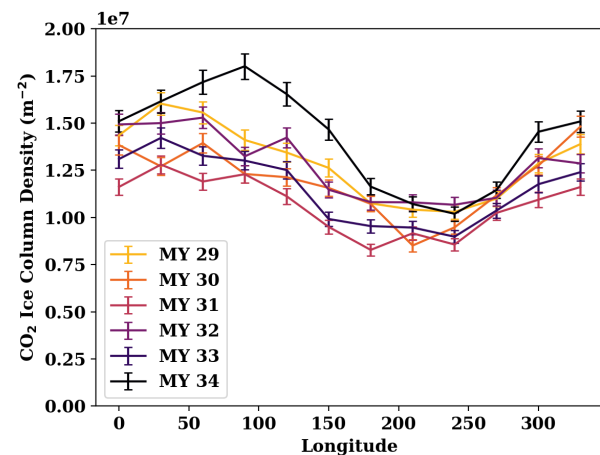


**Figure 3:** Winter CO<sub>2</sub> ice cloud column densities as a function of longitude. The column densities span 10 to 60 km above the polar surface and are averaged over 80° – 90° N for the entire winter season  $L_s$  180° – 360° of each year.

**Acknowledgements:** Part of this work was supported by NASA through the MRO project and by the United Arab Emirates Mohammed bin Rashid Space Center through support for N. R. Alsaeed.

**References:** [1] Waugh, D. W., et al. (2016) *JGR: Planets* 121(9) 1770-1785. [2] Mitchell, D. M., et. al. *JRMS*, 141(687), 550-562. [3] Forget, F., and Pollack, J. B. (1996). *JGR*, 101(E7), 16865-16879. [4] Leighton, R. B., & Murray, B. C. (1966), *Science*, 153(3732), 136-144. [5] Pollack, J. B., et al. (1990), *JGR*, 95(B2), 1447-1473. [6] McCleese, D. J., et. al. (2007), *JGR*, 112(E5). [7] Kleinböhl, A., et al. (2009), *JGR*, 114(E10). [8] Gary-Bicas, C. E., et. al. (2020). *JGR*, 125(5). [9] Hayne, P. O., et al. (2014), *Icarus*, 231, 122-130. [10] Millour, E., et. al. (2018), *From Mars Express to ExoMars*, 68. [11] Wilson, R. J. (1997). *GRL*, 24(2), 123-126. [12] Guzewich, S. D., et. al. (2016). *Icarus*, 278, 100-118. [13] Kass, D. M., et. al. (2016). *GRL*, 43(12), 6111-6118. [14] Banfield, D., et. al. (2003). *Icarus*, 161(2), 319-345.